Real-time Force Reconstruction in a Transverse Dynamic Force Microscope

Kaiqiang Zhang, *Member, IEEE*, Thang Nguyen, Christopher Edwards, *Senior Member, IEEE*, Massimo Antognozzi, Mervyn Miles, and Guido Herrmann, *Senior Member, IEEE*

***Abstract*—One major functionality of force microscopes is their ability to measure forces at a high sensitivity, thereby, allowing understanding of vital mechanisms: for instance, in bio-specimens. The investigation of a specimen's viscoelasticity on nano-scale can have significant scientific impact, but has been inhibited by the lack of fast, comprehensive scanning instruments. In principle, transverse dynamic force microscopes (TDFMs) permit the measurement of interaction forces within delicate samples in a non-contact manner. The force measurements are reconstructed via complicated offline analysis in TDFMs, therefore, they can hardly be utilised as an online force measuring tool. This paper introduces a novel integrated robust design for practical *scanning* using the TDFM system. The digital design is implemented in fixed-point arithmetic using Field Programmable Gate Array (FPGA) devices, thereby, permitting measurement of the interaction force at a high sampling rate. The novel digital design tackles different implementation issues achieving fast and robust force measuring performance. This enables a new *force-scan mode* for the TDFM, realising for the first time, online force mapping of sample-surfaces in real-time.**

***Index Terms*—Digital filters, Mechatronics, Nanotechnology, Observers, Parameter estimation, System dynamics, Scanning probe microscopy**

I. Introduction

THE invention of the Atomic Force Microscope (AFM) allows imaging samples at nano-meter precision [1]. AFMs play an important role in investigating physical phenomena [2], chemical reactions [3], material properties [4] and biological mechanisms [5] via measuring interaction-forces at a high sensitivity. For example, the interaction force, which occurs between cell-specimens and the cantilever-tip in a typical AFM device, can be measured and processed for analysing the mechanical properties, such as viscoelasticity, over sample surfaces [5]–[8]. Such techniques allow for investigating different diseases, such as cancer, arthritis, etc., by observing the variations in the samples' mechanical properties, which cause changes in the cell functionalities. Also, mechanical property changes can significantly contribute to an improved understanding of virus-shell properties, thereby, giving insight into virus assembly or disassembly mechanisms [9]. For these reasons, there has been significant research interest in developing and employing different approaches to measure the interaction forces using AFMs in the last decades.

The shear force microscope (SFM) [10], employs a vertical cantilever-probe which is excited horizontally. The vertical probe interacts with a confined liquid layer covering the sample-substrate without the need for directly contacting the sample surface. This sensing mechanism allows for true non-contact force measurement over the sample surface, thereby, avoiding damage to samples. In contrast, for a typical AFM, an appropriate contact force, determined by skilled experienced users, needs to be applied to the sample surface by the cantilever-tip, probably resulting in destructive damage to delicate samples [5], [11].

The special feature of non-contact scanning makes SFMs a powerful tool in force detection and sample analysis applications. For instance, SFM's can be used to measure the non-contact friction force between the cantilever and sample surfaces in [12]. The non-contact friction force is then reconstructed offline from the cantilever's dynamic measurements, such as displacement and velocity. Similarly, the amplitude and frequency changes in the cantilever oscillation are measured in [13] using a transverse dynamic force microscope (TDFM): a specific highly force-sensitive SFM invented at Bristol.

In TDFMs, the oscillating cantilever can work as a force sensor directly, by placing the cantilever in the sample solutions [2], [14], [15]. The interaction shear-force can be reconstructed via different numerical methods, thereby, allowing analysis of the viscous and elastic constants of different sample liquids. However, previously, the force measurements have been *reconstructed via offline data processing procedures* in these applications. The data analysis procedure is also time-consuming and requires very specific expertise.

Motivated by the need to carry out rapid force measurement in a non-contact manner, a feasible solution is to reconstruct the interaction force in TDFMs via force estimation algorithms. Although similar concepts have been applied to tapping mode AFMs [16], [17], these algorithms have not been feasible to be deployed in TDFMs due to the differences in the set-up. Specifically, a TDFM probe continuously interacts with the very top-layer of the specimen at each imaging position during specimen scans. This interaction guarantees that the specimen is only traversed above the surface. In contrast, a tapping mode AFM contacts or approximates the specimen during a short

Manuscript received Mar, 2021; revised Jun, 2021; accepted Aug, 2021. This work was conducted with the support of a University of Bristol Postgraduate Research Scholarship and EPSRC grants EP/I034882/1 & EP/I034831/1.

K. Zhang, M. Antognozzi and M. Miles are with the University of Bristol, BS8 1TL, UK.

T. Nguyen is with Texas A&M University - Corpus Christi, Corpus Christi, Texas 78412, USA. He is also affiliated with Thuyloi University, Hanoi, Vietnam.

C. Edwards is with the University of Exeter, EX4 4QF, UK.

G. Herrmann is with the University of Manchester, M13 9PL, UK (corresponding author with e-mail: guido.herrmann@manchester.ac.uk).

period in each oscillation period. For TDFMs, a theoretical framework is developed in [18], proposing a two-inputs-single-output model of the cantilever: one of the inputs is the known cantilever excitation, the other input is the unknown interaction shear force at the tip of the cantilever, and the output is the measurable cantilever oscillation motion in the complex scan medium. In particular, a suitable solution that estimates the interaction force using a sliding mode observer is discussed and analysed in [18], [19]. The recent work [19] succeeds in estimating the unknown shear-force input by processing practical data for specific points on the specimen using a separate data processing PC.

This paper presents a novel integrated solution for the TDFM system *achieving real-time force scans*, in contrast to the result of [19] which were obtained at fixed points on the specimen. Developed from previous work [19], a new implementation procedure is presented in this contribution, considering different practical issues. As a result, this novel design can integrate the real-time force measuring function with the multi-mode TDFM system [20]. A significant challenge is that the TDFM is expected to excite the cantilevers at the scale of hundreds of kilo-Hertz, which is higher than the existing experimental force observers in other AFMs [16], [17]. Therefore, the filters and numerical computations are implemented using fixed-point arithmetic, allowing the implementation of complex algorithms at Mega-Hertz level sampling frequencies on Field Programmable Gate Array (FPGA) boards. The force observer is modified for ease of FPGA implementation. A novel digital FPGA programme is carefully designed and parametrically optimised for a high numerical accuracy taking the hardware limitations into account. Experimental results are provided demonstrating the first real-time force-scan of nanoparticles in a non-contact manner using a TDFM.

It will be shown that the developed force-measurement functionality allows the TDFM to undertake shear-force scans and viscoelasticity analysis of samples in practice. This permits online analysis of the sample surface rapidly, whilst other methods compute the interaction force or the elastic/viscous constants of the scanning surface offline [21], [22]. Such functionality prospectively allows for online mapping the viscoelastic properties of the surface during biological or chemical processes of a specimen. In contrast, previously, only topographic images have been scanned online [23], [24]. Thus, this new real-time force reconstruction function makes the TDFM a powerful force measurement tool to detect and measure small forces at a high speed with the sensitive TDFM-probe, whereas rapid force changes due to physical phenomena (e.g., [25]) were not directly measurable before. Such capability contrasts and complements the force measurements of AFMs with a horizontal cantilever design, operated in a torsional mode [26], [27]. Specifically, in these AFMs, the torsional vibration of the excited cantilever interacts with the sample-substrate surface in lateral directions, when the cantilever-tip is vertically pressed against the sample-substrate in a contact regime. Although a carefully calibrated torsional AFM can be used to measure the lateral interaction forces for sample surface analysis, the lateral force is typically in the range of a few to several dozen nNs. In contrast, the presented TDFM interacts with the sample-substrates in a much smaller force range (e.g. in this work, the largest force levels are at about 0.2 nN) and extracts viscoelastic information from non-contact interaction over the sample surfaces.

II. Shear Force Reconstruction Formulation

A. Shear-force interaction modelling in the TDFM

A typical sample-substrate is commonly covered by a confined liquid layer in a scan medium, or a confined water layer, due to humidity in an ambient environment. This is specifically exploited in TDFMs. In this work, all the specimens are in water-based scan medium. As shown in the schematic in Fig.1, the cantilever can be assumed to be an Euler-Bernoulli bending beam [28]. The beam is excited at the upper end of the cantilever by a translation $u(t)$ in the oscillation direction at time t. Subsequently, the cantilever tip freely oscillates with transverse displacement $y_c(\xi, t)$ in the scan medium. There is no specific shear-force created on the cantilever tip when the cantilever is outside the shear force interaction range, i.e., the existing range of the confined water-layer over the sample-substrate. Here, ξ indicates the position value, along the beam (i.e. along the z-axis), starting from the upper end of the cantilever. As soon as the cantilever tip penetrates the confined water layer, the ordered water-molecule layer creates the shear force $f(t)$ in the opposite direction to the cantilever deflection along the y-axis.

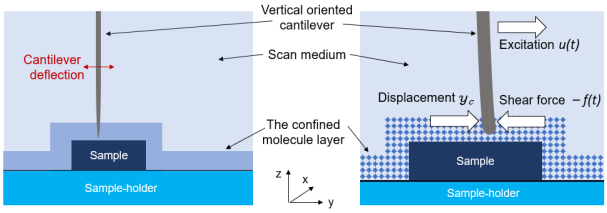

Fig. 1: A schematic of the cantilever oscillation modelled as a bending beam oscillating in the y direction. The beam is excited by $u(t)$ at the upper end and the shear force $f(t)$ is created due to the interaction with the confined water layer. The beam displacement y_c is the result of $u(t)$ and $f(t)$ together. The water-layer exists in a lattice structure and varies with different factors [2]. The simplified shape of the water-layer does not reflect any true measure in this schematic.

Based on the well known Euler-Bernoulli equation from beam theory, the partial differential equation is given as [28]:

$$EI\frac{\partial^4}{\partial \xi^4}(y_c + \alpha\frac{\partial y_c}{\partial t}) + \rho A_s\frac{\partial^2 y_c}{\partial t^2} + \gamma d\frac{\partial y_c}{\partial t} = 0 \qquad (1)$$

where the boundary conditions of the cantilever at time t are $y_c(\xi = 0) = u(t)$, $\frac{\partial y_c}{\partial \xi}(\xi = 0) = 0$, $\frac{\partial^2 y_c}{\partial \xi^2}(\xi = L) = 0$, $EI\frac{\partial^3 y_c}{\partial \xi^3}(\xi = L) = -f(t)$. Here, α is the internal damping constant added to represent the dissipative internal damping force, E is Young's modulus of the cantilever material, I indicates the second moment of area, A_s is the cross-sectional area of the cantilever, ρ is its density, γ is the viscous coefficient (Nsm^{-3}) of damping in the term $\gamma d\frac{\partial y_c}{\partial t}$ representing the

dissipative force caused by the surrounding environment, d is the width of the cantilever, and L is the cantilever length.

Specifically, the force $f(t)$ caused by the confined liquid layer can be separated into a viscous force and an elastic force:

$$f(t) = -\nu \frac{\partial y_c}{\partial t}|_{\xi=L} - \kappa y_c|_{\xi=L} \tag{2}$$

where ν is the constant of dissipative interaction (viscous damping coefficient ν) and κ is the elastic interaction constant (elastic spring coefficient κ) [28].

In TDFMs, the length of the cantilever is typically much greater than its thickness. Specifically, the adopted cantilevers are 18 μm in length in comparison with its 200 nm thickness. Moreover, the thickness of the confined water layer just above the specimen is commonly less than 10 nm, significantly smaller than the length of the cantilever. Therefore, equation (1) can be written in the given format without the need to consider the rotatory inertia and the effect of the shear force along a stretch of the cantilever. The cantilever deflection y_c depends on the position ξ and time t. The cantilever excitation $u(t)$ is a constant sine-wave oscillation provided by a dither piezo-actuator in the TDFM (see the set-up in Fig.2).

As $f(t)$ and $u(t)$ are not collocated, a cantilever model needs to be established to relate the system inputs $u(t)$, $f(t)$ and the output $y(t)$ allowing the estimation of the unknown shear-force signal $f(t)$ using an unknown input observer based only on the knowledge of $y(t)$ and $u(t)$. Here, the method of lines is used to approximate the partial differential equation (1) by time-invariant ordinary differential equations as introduced in our previous work [19]. This approach also retains some of the versatility of the partial differential equation, as forces and the scan-medium interferences can be modelled with good accuracy by choosing for instance the model parameters γ and α. Most importantly, this approach will provide an accurate control engineering perspective on the influence of the unknown shear force, $f(t)$ (and also the excitation signal $u(t)$) on the output $y(t)$, and the chosen observed states of the system. The process for obtaining this model is to first conduct a method of lines and then to use an established model reduction approach to obtain a good low order approximation of the dynamic relationship.

The linear time invariant system model of the cantilever can be written in a state space form as

$$\begin{aligned} \dot{x_l} &= A_l x_l + B_l u + D_l f \\ y_l &= C_l x_l \end{aligned} \tag{3}$$

where $x_l \in \mathbb{R}^{2(n-4)\times 1}$, $B_l =\in \mathbb{R}^{2(n-4)\times 1}$, $D_l \in \mathbb{R}^{2(n-4)\times 1}$ are computed from (1) using the method of lines detailed in [19]. Assuming n is sufficiently large (i.e. $\delta\xi \to 0$), the cantilever deflection y_l can be approximated by the $(2n-9)$th entry of x_l. Hence, the $(2n-9)$th entry of $C_l \in \mathbb{R}^{2(n-4)\times 1}$ is 1 and the remaining entries are zero.

The dynamic model (3) is often expressed by a high order state-space model, as the number of nodes n needs to be sufficiently large. This potentially results in a high order force estimator, that cannot be successfully implemented on digital hardware with limited hardware resource, particularly FPGA boards. In order to guarantee the implementability, a standard balanced truncation method [29] is applied to the high order state space model. Practically, it has been found an 8th order state space model can well approximate the high-order state-space model. The order reduced model is represented by

$$\begin{aligned} \dot{x}(t) &= Ax(t) + Bu(t) + Df(t) \\ y(t) &= Cx(t) \end{aligned} \tag{4}$$

which will be used to design the unknown input, force $f(t)$, estimator. Here, the cantilever tip displacement is represented by $y(t)$ (= $y_c(\xi, t)|_{\xi=L}$). Note that the reduced model has to be carefully calibrated to agree with the cantilever dynamics in practice for accurate force reconstruction (see the detailed procedure described in Section III-C).

B. Observers for force reconstruction

Here, inspired by previous results [19], a sliding mode observer is designed for estimating the interaction shear-force in real-time:

$$\begin{aligned} \dot{\hat{x}}(t) &= A\hat{x}(t) + Bu(t) + D\phi + G(y(t) - \hat{y}(t)) \\ \hat{y}(t) &= C\hat{x}(t) \end{aligned} \tag{5}$$

where G is a gain matrix and $\hat{x}(t)$ is the estimation of $x(t)$. In (5), $\hat{y}(t)$ denotes the estimated tip oscillation signal and ϕ is the nonlinear injection signal defined as

$$\phi = \begin{cases} -\Lambda sign(\hat{y}(t) - y(t)) & \text{if } |\hat{y}(t) - y(t)| \geqslant 1 \\ -\Lambda(\hat{y}(t) - y(t)) & \text{if } |\hat{y}(t) - y(t)| < 1 \end{cases} \tag{6}$$

and the $sign(\cdot)$ is the mathematical operation to take the sign of the input variable. This can be realised by multiplying the saturated signal $\hat{y}(t) - y(t)$ with a [-1,1] range, by $-\Lambda$. Here Λ represents a positive scalar gain satisfying

$$\max(\|f(t)\|) < \Lambda. \tag{7}$$

The previous single-position results [19] show that, for an appropriate choice of G and the scalar Λ, the output estimation error $\hat{y}(t) - y(t)$ is driven to a neighbourhood of zero in finite time and a so-called pseudo sliding motion takes place [30]. Here, a practical design chooses G as a zero matrix, $G = \mathbf{0}$. Thus, it follows the design approach as analysed in [30].

Following Section 6.2 and Proposition 6.2 in the work in [30], necessary and sufficient conditions for the existence of this observer are:

1) The matrix A is Hurwitz, i.e. stable, in the left half plane;
2) $CD \neq 0$, i.e. the model (A,D,C) is relative degree one;
3) The invariant zeros of (A,D,C) are stable, i.e. the zeros of the transfer function $C(sI - A)^{-1}D$ are stable.

Practically, the first condition is always satisfied for the cantilever. The second and third conditions are generally guaranteed through the practically guided model order reduction process, where stable zeros and a relative degree one transfer function for $C(sI - A)^{-1}D$ is enforced.

Given $G = \mathbf{0}$, the force estimator is realised as

$$\begin{aligned} \dot{\hat{x}}(t) &= A\hat{x}(t) + Bu(t) + D\phi \\ \hat{y}(t) &= C\hat{x}(t) \end{aligned} \tag{8}$$

where ϕ is defined in (6). Such an implementation has two significant advantages. The first benefit is that G is not needed.

Otherwise, the design of G would have to be robust to changes in the system (e.g. a slight change of the optical sensitivity), i.e., it therefore increases the difficulties to use the TDFM as a force measurement tool. Moreover, the absence of the multiplication of two matrices saves significant digital design effort and hardware computational resource.

Formally, during the sliding motion, on average, the high frequency switching term ϕ must replicate $f(t)$ for sliding to be maintained. The average value of $-\phi$ necessary to maintain sliding is known as the equivalent injection [30]. Since $\hat{y}(t) - y(t) \to 0$ as $t \to \infty$ due to the convergence, the negative value of the equivalent injection will be equal to $f(t)$.

The successful estimation of $f(t)$ provides information about the viscous damping coefficient $\nu(t)$ and elastic spring coefficient $\kappa(t)$ based on the dynamics (2). Here, the mechanical properties of the specimen surface, specifically ν and κ, vary during a dynamic scan. Hence, an unknown parameter estimation algorithm developed in [31] is selected, which gives a robust adaptive parameter estimation performance. In detail, equation (2) is rewritten as

$$\begin{aligned} f &= \begin{bmatrix} \dot{y} & y \end{bmatrix} \begin{bmatrix} -\nu \\ -\kappa \end{bmatrix} \\ &= \Psi(t)\Theta \end{aligned} \tag{9}$$

where $\Psi = \begin{bmatrix} \dot{y} & y \end{bmatrix}$ and $\Theta = \begin{bmatrix} -\nu & -\kappa \end{bmatrix}^T$. A simple first order filter is introduced for each term of (9) in the form:

$$\begin{aligned} k\dot{f}_f(t) + f_f(t) &= f(t), \qquad f_f(0) = 0 \\ k\dot{\Psi}_f(t) + \Psi_f(t) &= \Psi(t), \qquad \Psi_f(0) = 0 \end{aligned} \tag{10}$$

The application of $\Psi_f(t)$ filters to $y(t)$ for calculating $y_f(t)$ enables obtaining $\dot{y}_f(t)$ according to

$$k\dot{y}_f(t) + y_f(t) = y(t), \qquad y(0) = 0. \tag{11}$$

This $\dot{y}_f(t)$ is taken as $\dot{y}(t)$ instead of directly computing the derivative of $y(t)$. The filtered version of (9) is written as $f_f = \Psi_f\Theta$, assuming that the change in parameter value κ and ν in relation to the following regressor filter operation is slow and κ and ν can be regarded as (almost) constant.

Two filtered regressors $M(t)$ and $N(t)$ are formulated as

$$\begin{aligned} \dot{M}(t) &= -lM(t) + l\Psi_f^T(t)\Psi_f(t), \qquad M(0) = 0 \\ \dot{N}(t) &= -lN(t) + l\Psi_f^T(t)f_f(t), \qquad N(0) = 0 \end{aligned} \tag{12}$$

where l is a positive scalar, acting as a forgetting factor in this first order filtering process. The time constant, $1/l$ provides an approximate time interval during which κ and ν are estimated. Hence, the factor l is typically selected as a large number for a fast convergence speed, whereas an extremely large l should be avoided, to guarantee sufficient data for the computation of κ and ν. For instance, in practice, l is configured to be 1.885×10^4 to average the data in a relatively long period of about 0.3 ms. In this way, sufficient data is fed into the parameter estimator for an accurate estimation of the viscous damping coefficient ν and the elastic spring coefficient κ, considering the cantilever oscillation at 200 kHz and a 4 MHz sampling rate of the force measurement (see the digital design details in Section III). Notice that $\dot{y}(t)$ and $f(t)$ are filtered and estimated from the measured and filtered value of $y(t)$. Thus, the estimation of $\Theta = \begin{bmatrix} -\nu & -\kappa \end{bmatrix}^T$ is given by

$$\hat{\Theta} = M^{-1}N. \tag{13}$$

The presence of sufficient data (e.g. persistency of excitation) within the period of length, $1/l$, in the formulation of $M(t)$ and $N(t)$, guarantees $\hat{\Theta} - \Theta \to 0$ in finite time [31]. The matrix-inversion formulation provides a lightweight and effective estimator for ν and κ, thereby, allowing the estimation of the viscous and elastic forces. Note that the online estimation of ν and κ can be realised using a variety of parameter estimation algorithms. Here, it is realised by a robust, light-effort estimation algorithm (10)-(13), motivated by the need for low computational cost and fast computation speed.

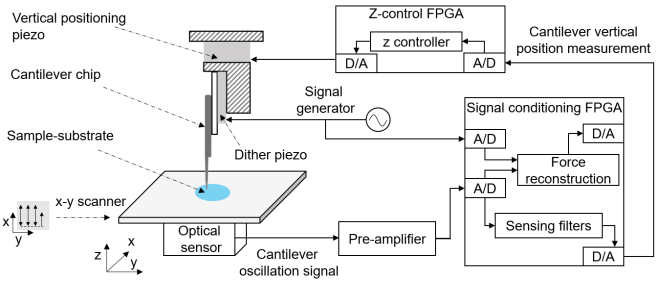

Fig. 2: A schematic of the vertical positioning and sensing components in the integrated TDFM system. Here, A/D and D/A indicate analogue-to-digital and digital-to-analogue channels respectively.

III. Integrated FPGA Design and Implementation

A. Real-time force observer in the TDFM System

The integrated TDFM system [20] consists of two FPGA modules for vertical positioning control in the z-axis (as shown in Fig.2). The x-y scanner carries the transparent sample-holder, as it moves along a raster trajectory in the TDFM scans. In particular, the fast and slow raster motion is along the x-axis and y-axis, respectively.

The cantilever is excited by a dither piezo-actuator in the TDFM. It only needs a small cantilever excitation $u(t)$ at a constant frequency so that the oscillation amplitude of the cantilever tip is small enough for a high spatial resolution. The cantilever excitation $u(t)$ can be computed from the sinusoid signal (generated from a signal generator) via a linear relationship. The cantilever deflection $y(t)$, measured by the optical sensor (see the optical sensing mechanism in [32] and the associated control design in [20]), is amplified before being processed by a signal conditioning FPGA module, a National Instrument NI-7962R FPGA. Consequently, the optical sensor provides two vertical position measurements which are used by the z-control FPGA, an NI-7854R, employing the vertical positioning piezo-actuators. In detail, the system [20] allows for measuring a relative position (the cantilever-sample interdistance within the shear-force interaction range) and an absolute position (the distance measured from the sample-holder slide) of the cantilever.

Here, the integrated control design includes two FPGA modules for several practical considerations. Specifically, the signal conditioning FPGA has a sufficiently high Input/Output (IO) sampling rate, allowing the processing of the cantilever oscillation measurement at a few mega-Hertz (as detailed in the next sections). In contrast, the z-control FPGA has a less powerful IO running at a relatively low sampling rate of 500 kHz, which is enough for the cantilever's vertical positioning with a control bandwidth below 10 kHz. Due to the limited amount of hardware resource (binary gates) on each FPGA boards, it is impossible to load the sensing functions and the vertical positioning functions onto one FPGA module. Therefore, the advanced digital controllers are implemented on the NI-7854R and occupy almost all hardware resource of the z-control FPGA [20]. On the other hand, the NI-7962R FPGA, the signal conditioning FPGA, is adopted for implementing the shear-force reconstruction function in addition to the vertical position sensing function (see Fig.2). This design integrates the real-time force-measurement function into the TDFM system, thereby, enabling an additional force-scan mode of the multi-mode force microscope presented in Section IV.

B. FPGA implementation using fixed-point arithmetic

In the field of AFM control, the typical method to prototype control algorithms at high clock frequencies on FGPAs is by implementing numerical operations in fixed-point arithmetic, e.g., [20], [33]. A significant challenge is that the digital programmes on FPGAs have to be carefully designed to achieve an appropriate performance, limited by different practical constraints, such as the finite amount of FPGA hardware resource. The real-time force estimation is implemented on the NI-7962R, as shown in Fig.3, taking into the consideration the following design issues.

The synchronisation of the system inputs $u(t)$ and $y(t)$ is critical for an accurate force estimation performance. In particular, the sinusoid signal from the signal generator is acquired as the U_{in} signal. The cantilever deflection signal is captured as the Y_{in} signal from the pre-amplifier. The measured Y_{in} is always delayed by the electronics, mainly the optical sensor and the pre-amplifier. Hence, a delay programme is suggested to accurately synchronise u and y. Specifically, the input A/D channels and the delay block are configured at the highest available sampling rates, therefore, the digitisation effect on signals is minimised. The digital delay is manually adjustable for the u signal subject to the minimum delay step of 5 ns.

The presence of measurement noise considerably influences the estimation precision in practice. The noise mainly consists of high frequency electro-magnetic noise inherent from the electronics and the spiky noise caused by the A/D conversion (running at the maximum rate of 100 MHz). To reduce noise, two bandpass filters are applied to both the U_{in} and Y_{in} measurements. Then, the bandpass filtered signals are used as the inputs to the shear force observer. It is critical to guarantee the filtered u and y are modified by the same gain and phase. Hence, identical filters are designed as 2nd order butter-worth filters with 180-220 kHz bandwidths covering the oscillation frequencies cantilever in the scan medium.

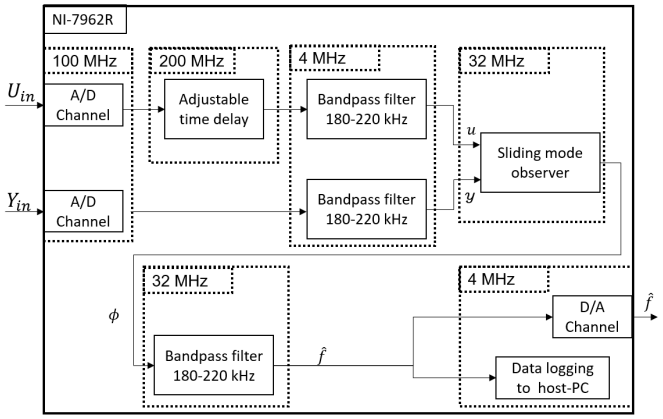

Fig. 3: The digital design of the force reconstruction function in the signal conditioning FPGA.

Note that an adjustable gain is introduced to the filtered Y_{in}. In practice, the optical sensitivity slightly alters as the optical path changes due to different experimental factors, such as the change of the sample-holder. Therefore, the gain for computing y is designed to be online adjustable. This design flexibility avoids spending hours reconfiguring FPGA programmes when the experimental condition slightly alters. On the other hand, the use of an adjustable gain slows down the running speed of the aforementioned bandpass filters. Specifically, the two filters are configured to run at 4 MHz, and that is a sufficiently high sampling rate for the shear-force reconstruction.

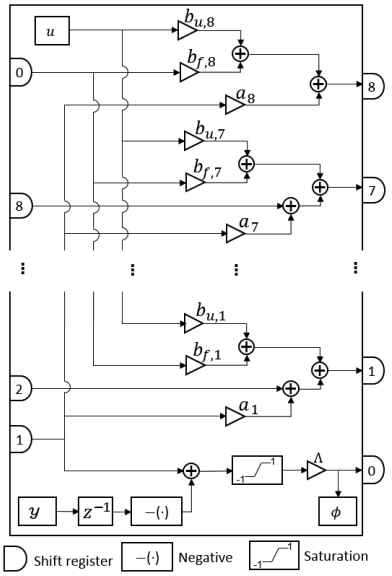

Fig. 4: The digital design of the sliding mode observer to be implemented on FPGA. The estimator in (14) is realised in a modified Transposed Direct Form II. The injection ϕ is computed by the inputs u and y according to the sliding mode observer design of (8). Specifically, a single clock cycle delay is applied to y as the $\hat{y}$ is delayed by one clock-cycle to calculate the estimation error.

The structure of the estimator has to be carefully designed

to manage the complex digital filtering function running at a fast sampling time. The result of [19], focussing on a single point, used the collected data to run the algorithm in the associated PC within a continuous-time numerical process. As a result, the state space representation of (5) allowed matrix-multiplication and continuous-time integration of $\dot{x}$. However, a direct, more complete, implementation on the FPGA is practically infeasible. Hence, the estimator in (8) is therefore discretised by using Tustin's method, and transformed into observable canonical form. The estimation of $y(t)$ in discrete time is given as

$$\hat{Y}(z) = \frac{\sum_{k=1}^{8} b_{u,k} z^{-k} U(z) + \sum_{k=1}^{8} b_{f,k} z^{-k} \Phi(z)}{1 + \sum_{k=1}^{8} a_k z^{-k}} \quad (14)$$

where $\hat{Y}(z)$, $U(z)$, and $\Phi(z)$ are the discretised z-transforms of $y(t)$, $u(t)$, and $\phi(t)$. To implement the observer with minimal hardware cost at a high running speed, the estimation $\hat{y}(t)$ is implemented by fixed-point arithmetic in a modified Transposed Direct Form II (TDF-II) structure (see Fig.4). Specifically, the value buffered in shift register 1 is added to the delayed negative value of y. Whilst this one cycle delay is not necessarily needed in a typical TDF-II digital filter implementation, here it permits carrying out the fixed point operations, the multiplication with λ and the saturation operation for computing the nonlinear injection signal ϕ, in parallel to other primary digital filtering computations. Also, this implementation structure allows the digital programme to execute the filtering computation in parallel at one clock cycle time, which is usually implemented as a series of computational elements (including one multiplication and two addition computations). The specific design achieves practically a 32 MHz sampling frequency, which maximises the performance of the parallel implementation of the complex high-order sliding mode filtering.

The fixed-point arithmetic operations of the digital filters have to be carefully designed in order to guarantee sufficient computational accuracy. The multiplication and addition operations implemented on the FPGA board have fixed numerical accuracy and range. The zeros and poles of the high-order estimator are sensitive to quantisation errors. Also, overflows have to be avoided by enlarging the numerical range of each arithmetic operation. Moreover, both design requirements, reducing the quantisation error and increasing the numerical range, need to be designed considering the limited hardware resource of the FPGA board, for which a solution will be discussed in the next section.

The previous single-position results of [19] demonstrate that a simple first order low-pass filter applied to $-\phi$ can provide a good force estimation $\hat{f}(t)$. However, the hardware limitation, particularly, the insufficient sampling rate of the injection, introduces quantisation errors/noise to $\hat{f}(t)$ over the whole frequency range. Practically, the signal $f(t)$ is created by the tip oscillation determined by the excitation $u(t)$, i.e. $f(t)$ mainly oscillates at the same frequency of $u(t)$. Hence, a bandpass filter is suggested to obtain the shear force information at the particular frequency, and additionally reduce the noise caused by quantisation errors. A 5th order Butterworth bandpass filter was used in order to achieve good estimation performance at low computational resource cost.

The design of the real-time shear force estimator is shown as Fig.3. Each of the functional blocks are implemented to run in parallel for maximising the overall implementation rate of the estimation scheme. A 4 MHz data logging and D/A output rate is chosen, due to the speed limitation of the data streaming from the FPGA towards the host-PC. For efficient data streaming and to avoid data loss, the data-logging function is designed as a dual-layer mechanism: a buffer to extract data from the FPGA's digital cache to the host-PC RAM at 1 kHz running rate, and a buffer to stack data from the RAM to a data-presenting functional thread running at a 25 Hz speed. At the host-PC side, the real-time force measurement can be imaged as a force-scan of the sample surface directly. Then, the force data can be processed into viscosity and elasticity data of the sample surface, via the proposed parameter estimation algorithm (presented as (10), (12), and (13)).

C. Practical implementation procedure

In order to facilitate the estimator, a practical model in the format of (4) has to be obtained taking into account various implementation factors, e.g. the amplifiers, the electronics, etc. The FPGA programme has to be optimised for achieving appropriate numerical precision before being deployed onto FPGA boards. Then, an estimator designed for the practical model is feasible to be implemented and used for the real-time force measurement. Here, a complete implementation procedure is suggested as given in the following steps:

- Identify the $u(t)$-to-$y(t)$ response of the cantilever oscillation outside the shear force interaction range.
- Adjust the parameters of the theoretical state-space model (3) to match the practically identified system dynamics (so that the fitted model is a practical model for the estimator design).
- Reduce the fitted state-space model into the low-order format of (4) retaining the critical dynamics information around the cantilever oscillation frequency.
- Compute the order-reduced cantilever model (4), discretise it, and then transform the discrete model into (14).
- Optimise the fixed-point arithmetic in the digital programme before deployment onto the FPGA board.

Here, an example is described with the experimental specifications in this work so as to demonstrate the whole implementation procedure. Specifically, the adopted cantilever probe (NuNano Ltd.) is selected to be excited in the horizontal plane along the y-axis by a sine wave of amplitude approximately 2 nm at 200 kHz, which is around its first resonance in water.

The excited cantilever oscillation dynamics of $u(t)$-to-$y(t)$ is measurable only when there is no shear force interaction involved. Applying the swept sine method around the 200 kHz excitation frequency, the frequency response $Y(s)/U(s)$ ($U(s) = \mathcal{L}\{u(t)\}$, $Y(s) = \mathcal{L}\{Y(t)\}$) of the $u(t)$-to-$y(t)$ plant is measured when the cantilever is placed at 20 nm above the sample-holder slide to avoid the influence of the shear force. In practice, the identified frequency response has the

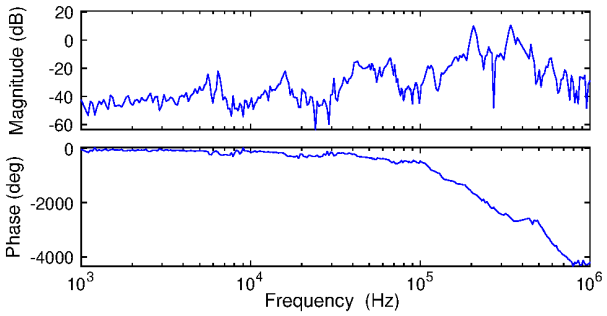

Fig. 5: Measured $Y(s)/U(s)$ dynamic response of the cantilever. The cantilever oscillation is caused by only an excitation without any shear-force interaction. The $Y(s)/U(s)$ plant has a first significant resonance around 200 kHz, i.e., the first resonance in water. Other mechanical components, related to the cantilever fixture, cause resonances (at about 5 kHz, 15 kHz, etc.) at a much smaller magnitude.

input U_{in} (excitation from the signal generator) and the output Y_{in} (optical data measurement from the photo-detector and then being amplified by the amplifier) in voltages (see Fig.5). Hence, the practical model needs to fit the plant response computed from the input and output signals. This guarantees that the subsequently designed estimator can be deployed on the hardware without extra adjustment. Note that the measured frequency response is computed from the input and output signals that have different units in relation to the theoretical high-order state-space model. This measured frequency response also contains the effects of amplifications. Therefore, a scaling factor needs to be applied to the theoretical model to ensure that the magnitude of the model fits the measured response.

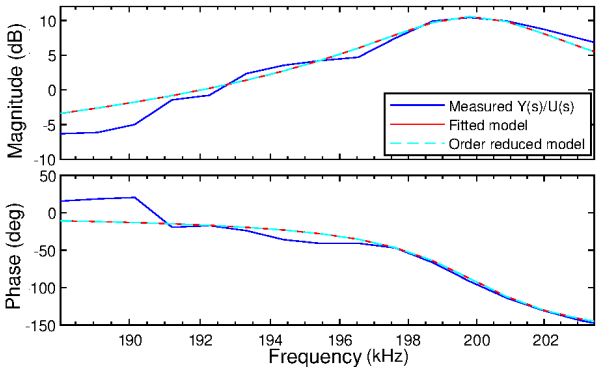

Fig. 6: The fitted high-order and the order-reduced cantilever models are adjusted to match the measured $Y(s)/U(s)$ frequency response around the resonance frequency in detail.

After the $Y(s)/U(s)$ response is practically measured for the cantilever, the linear time-invariant model (in the state space form of (3)) needs to be parametrically adjusted to fit the practical data. After deciding a sufficiently large n, the parameters α, γ, and the scaling factor are chosen to make sure the high-order state-space model fits the practically measured $Y(s)/U(s)$ response, while the other parameters are fixed specifications of the cantilever. Specifically, the parameters α and γ need to be adjusted to fit the theoretical model around the resonance (as shown in Fig.6). A two-step procedure can be applied here. First, the internal damping constant α is adjusted to fit the theoretical model of the cantilever to a measured $Y(s)/U(s)$ in an ambient environment, where $\gamma = 0$. Then, with α confirmed, the damping coefficient γ caused by its surroundings can be tuned by matching the theoretical model with the measured $Y(s)/U(s)$ in the specific scanning medium, e.g. the water buffer in this work. For example, this coefficient can be chosen following the damping coefficient tuning method given in [34]. Then, the scaling factor can be tuned (as suggested in [19]) by adjusting the magnitude of the theoretical model to fit the measured $Y(s)/U(s)$ response in the low frequency range, where the phase values are close to zero. In practice, it is possible to calibrate the gain from the actuation signal to the optical sensor's measurement (see Fig.2), when the optical sensor is optimised for a high sensitivity as a part of experimental preparation protocol [32]. Then, this calibrated gain can be multiplied by the known pre-amplifier gain as the overall amplification of the measured $Y(s)/U(s)$, i.e., the scaling factor.

The order reduced model (4) precisely matches the high-order state-space model as Fig.6 shows. Note that the cantilever only works at the excited resonance frequency in practice. Hence, the model needs to match the magnitude and the phase of the practical measurement around the excitation frequency. The state-space model of (4) is determined having the frequency response as shown in Fig.7, which is the practical model to be used for developing the force estimator and to be implemented in the TDF-II form of (14) on the FPGA.

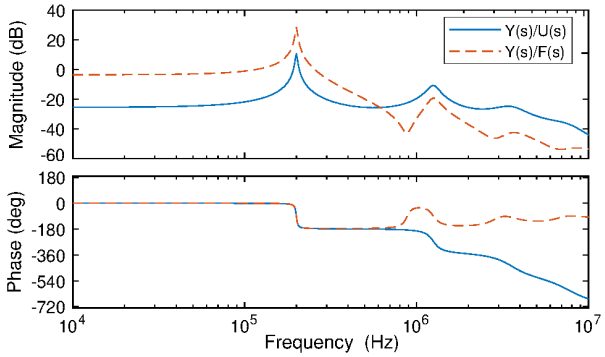

Fig. 7: The order-reduced cantilever dynamics model: $Y(s)$, $U(s)$, and $F(s)$ indicate the cantilever-tip displacement, excitation, and shear-force in the Laplace domain. Here, the dynamic models are scaled to fit the measured dynamic response in practice.

The digital design, in Fig.3, can be then optimised via the method introduced in [20]. Specifically, before practical implementation, the computational accuracy can be assessed by replicating the fixed-point design (as shown in Fig.3) in simulation. The replicated fixed-point based simulation is given a maximum feasible sampling rate of 32 MHz. Then, simulated signals $\tilde{u}$ and $\tilde{f}$ are given to a simulated cantilever dynamics model, outputting a mock cantilever oscillation $\tilde{y}$ in continuous time. The simulated $\tilde{y}$ and $\tilde{u}$ can be used by the

digital estimator simulation in fixed-point arithmetic to obtain the estimated force $\tilde{f}_e$. In the process, different fixed-point configurations of multiplications and additions are tested in the simulation to guarantee $\tilde{f}_e \rightarrow \tilde{f}$. The configured digital implementation is assessed by being compiled and deployed on the FPGA board, i.e. the off-line optimised programme is confirmed to be implementable considering practical hardware resource limitations. The optimised design is meant to have the minimal difference between $\tilde{f}_e$ and $\tilde{f}$ when the digital implementation can be compiled and loaded on the NI-7962R. As a result, the implemented force estimator provides the least magnitude of $|\tilde{f}_e - \tilde{f}|$, while the overall design may consume all hardware resources of the NI-7962R in terms of FPGA binary gates for fixed-point arithmetic operations.

IV. Force Reconstruction in Practice

The effectiveness of a sliding mode algorithm has been investigated in [19], therefore, this work focuses on demonstrating the performance of the novel integrated FPGA implementation in dynamic scanning tasks. The shear-force estimator is assessed under controlled experimental conditions of around $20°C$ and 50% humidity. The experiments show the shear-force measurement is achieved at a cantilever resonance frequency of 200 kHz frequency in real-time. This is the first time that a shear-force scan is carried out completely in real-time and in practice, and permits full specimen scans. The viscous and elastic constants of the sample-substrate surface are analysed by the host-PC at a slower speed.

A. Dynamic force measure in real-time

To verify the practical measurement noise, there is no sample placed on the sample-holder slide which is a grade 0 glass slide. The cantilever is placed at 20 nm away from the sample-holder surface outside the interaction region. At this distance, the estimator provides the real-time measurement caused by electro-magnetic noise and Brownian motion. It demonstrates that the system has a noise amplitude of about 0.03 nN shear force amplitude and a 0.02 nN rms (root mean square). Applying a fast-Fourier transformation via the fft function in Matlab, the amplitude of the noise signal at each frequency is smaller than 0.7×10^{-6} nN, which is ignorable with respect to the estimated force level of 0.001 nN.

The shear force estimator is then tested by the following dynamic assessments. The cantilever oscillates at 200 kHz with ∼2 nm amplitude when there is no shear-force interaction in water. The cantilever is initialised to be at ∼6 nm above the sample-substrate at the boundary of the shear-force interaction range. The cantilever is then controlled to move towards the sample-substrate following a 100 Hz square wave with a step-size of 5 nm. The results in Fig.8 show that the shear force estimator can measure a rapid shear-force amplitude change (ascending or descending) between 0.03-0.12 nN. As noise is a predominant factor in real-time measurement, the convergence time cannot be identified clearly. Because the closed-loop positioning system has a ∼0.25 ms settling time, an overall convergence time of the force reconstruction in less than 0.3 ms is achieved in practice.

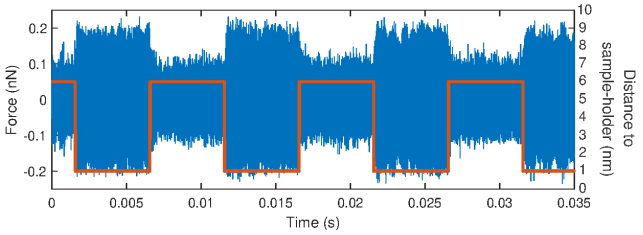

Fig. 8: The real-time shear-force measurement (in blue) when the cantilever is controlled (following the trajectory in red) to jump between 1 nm and 6 nm above the sample-holder slide at 100 Hz frequency in water.

At the initial position of ∼6 nm over the sample-substrate, the shear-force is measured when the cantilever continuously moves. The cantilever is controlled following a 100 Hz sine wave with a peak-to-peak value of 5 nm. The real-time shear-force is measured by the force estimator is presented in Fig.9a.

The estimated force is streamed to and then processed by the host-PC for further analysis. Applying the proposed estimator, the viscous damping ν and the elastic spring κ coefficients can be online measured as shown in Fig 9b. The host-PC is not capable of running the ν and κ observer in real-time because of the large volume of real-time data, so these results are obtained at a slower speed within a settling time of 0.6 ms in practice. The viscous and elastic forces are computed by the host-PC based on the real-time force measurement as shown in Fig.9c.

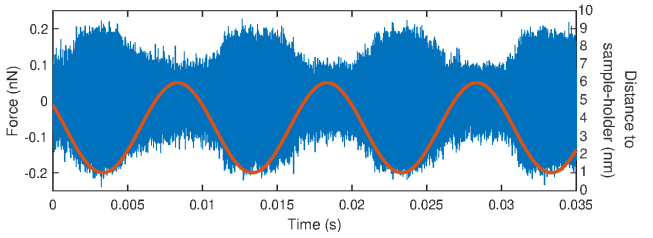

(a) Real-time shear-force measurement

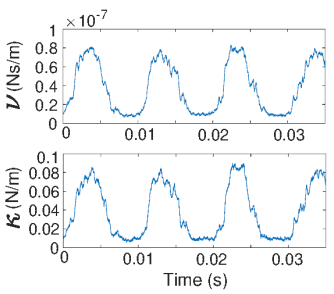

(b) Dynamic estimation of viscous damping and elastic spring coefficients

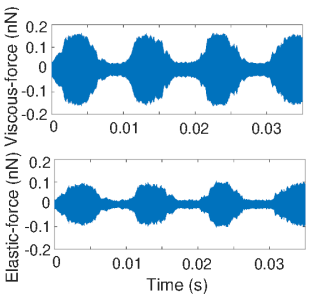

(c) Dynamic viscous and elastic forces estimation

Fig. 9: Measurement results when the cantilever is controlled to continuously move between 1 nm and 6 nm above the sample-holder slide along a sine trajectory at 100 Hz frequency in water: a) The real-time shear-force measurement (in blue) as the cantilever continuously moves along the sine trajectory (in red); b) Dynamic estimation of viscous damping and elastic spring coefficients; c) Dynamic estimation of viscous force and elastic force.

B. Novel force scan mode of the TDFM

In principle, the force-scan mode enforces a constant distance between the cantilever and the sample-holder slide. The real-time interaction shear-force is measured by the proposed shear-force estimator as the cantilever travels over the whole sample-substrate. The top bulges of specimens appear in the shear-force interaction range and result in a lower cantilever-specimen distance measurement obtained from the decreased cantilever tip-oscillation at those points; this is caused by an increased shear-force (see the interaction schematic in Fig.1). Thus, the TDFM allows for imaging the cantilever distance away from the specimen top bulges while retaining the cantilever at a constant distance from the sample-holder, i.e., implying the Constant Absolute Height (CAH) mode of the TDFM [20]). Importantly, the shear-force scan mode can be verified by comparison with a CAH scanning result in the same area. Note that the TDFM is designed to scan samples in a non-contact manner [20], permitting the imaging of fragile samples without damage. Therefore, the CAH scan mode and the presented force scan mode tend to be undertaken at an appropriate scanning height which avoids direct contact between the cantilever and the sample.

In experimental scans, a 20 μl nano-sphere sample solution is prepared and dropped on a grade 0 glass slide. Specifically, the sample solution is prepared in a pure water buffer with a 10 mM/L concentration of polymer microspheres (Fluoro-Max, Thermo Fisher Scientific Inc.) with a nominal diameter of 50 nm and a 10 mM/L concentration of $NiCl_2$, which creates salt bridges, bonding the nano-spheres to the sample-holder slide. Here, an 800 nm $\times$ 800 nm area is scanned in the CAH mode and then the force-scan mode, each at 50 nm above the glass slide at a resolution of 2 nm/pixel at a scanning speed of 1.6 μm/s. Hence, each pixel is measured in a period of 1.25 ms guaranteeing enough time for precise force/viscosity/elasticity measurement.

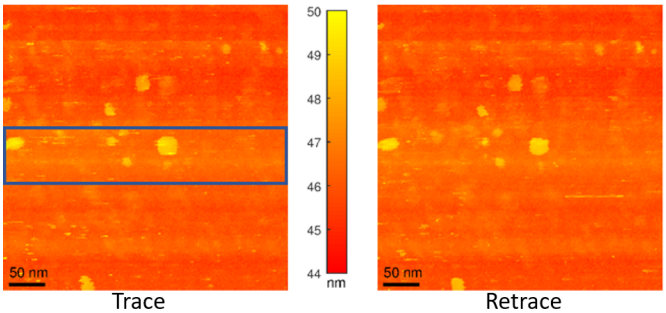

Fig. 10: A Constant Absolute Height scan is carried out in an 800 nm $\times$ 800 nm area at 1.6 μm/s speed and 2 nm/pixel resolution in water. The specimens are $\sim$50 nm diameter nano-spheres. The square area is scanned by the force-scan mode in comparison.

The CAH scan is shown in Fig.10. The nano-spheres within the framed area are then targeted to be scanned in the real-time force scan mode. The rms value of the force measurement is real-time imaged for this area as shown in Fig.11a. The interaction shear-force image in Fig.11a exactly matches with the CAH scanning result in Fig.10. The interaction shear-force

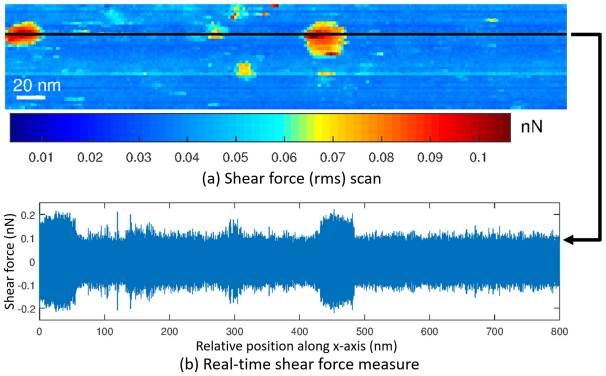

Fig. 11: The force-scan result of scanning $\sim$50 nm diameter nano-spheres in real-time: (a) is the rms of the interaction shear-force over the target area; (b) presents the detailed force measurement of a scanned raster (black) line during the scan.

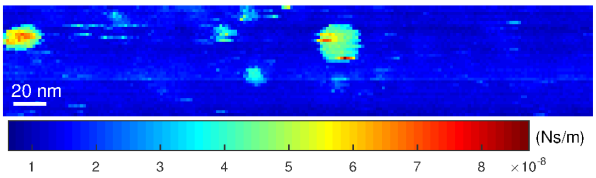

(a) Dynamic viscous damping coefficient measurement over the scanned area

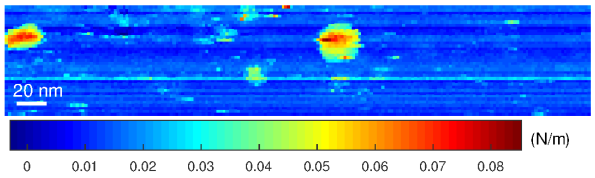

(b) Dynamic elastic spring coefficient measurement over the scanned area

Fig. 12: Viscous damping coefficient ν and elastic spring coefficient κ measurement over the focused scanning area.

is stronger as the specimens' top-parts enters more into the relative height sensing range of the specimens. This interaction force strength image gives an understanding of the dynamic interaction over a scanned area, i.e. this helps to analyse the dynamic mechanisms of biological specimen surfaces in real-time. Also, the detailed real-time shear force measurement as a function of time can be observed during dynamic scans. In detail, the shear-force measurement of a scanned raster-line can be monitored in real-time, e.g., the force measurement of the scanned (black) line in Fig.11a is presented in Fig.11b. This force reconstruction feature acts as a real-time shear-force sensor giving the time transient of the shear-force information.

The shear-force scan in Fig.11a is processed by the host-PC to analyse the elastic spring coefficient in Fig.12a and the viscous damping coefficient in Fig.12b over the nano-sphere top surface. The elastic and the viscous coefficient scanning results show high similarity over the whole scanned area with some obvious differences. Both coefficients increase with the increasing shear-force interaction agreeing with the

fixed single position measurement in Fig.9b. It can be seen that the elastic constant varies with the topographic height in a gentle manner at the sphere top in Fig.12a. In contrast, the viscous constant changes significantly over the nano-sphere surface, presenting a large area with high viscous coefficient values at the top of the target sphere in Fig.12b.

The scanning results demonstrate that the force scan mode allows online presentation of four kinds of information: a) the shear-force interaction strength over a scan area in real-time; b) the real-time transient shear-force measurement over a period of time during a dynamic scan; c) an online elastic spring constant scan of the confined hybrid layer over a specimen top; d) the viscous damping constant over a specimen top can be scanned online.

V. Conclusions

This paper presents an integrated design allowing real-time force-measurement in a TDFM. The novel design is implemented at a high-sensing bandwidth using fixed-point arithmetic in FPGA devices. The proposed design maximises the real-time performance of the FPGA programmes taking into consideration various practical issues. An implementation procedure describes the approach to configure the FPGA programmes for optimised performance. The integrated design permits the TDFM to measure the dynamic interaction force in real-time. As a result, the TFDM processes a novel real-time shear-force-scan mode, which permits the online identification of viscous and elastic material constants from a scan across the specimens' top. This feature gives insight to help understand the mechanical properties of the confined liquid layer, and physical mechanics/properties over specimen surfaces. Future work will focus on using the TDFM for rapid force measurement, verifying visco-elastic properties over sample surfaces, and investigating different samples in physics, chemistry, and bio-medical research.

References

[1] G. Binnig *et al.*, "Atomic force microscope," *Phys. Rev. Lett.*, 1986.

[2] M. Antognozzi *et al.*, "Observation of molecular layering in a confined water film and study of the layers viscoelastic properties," *Appl. Phys. Lett.*, 2001.

[3] N. Pavliček and L. Gross, "Generation, manipulation and characterization of molecules by atomic force microscopy," *Nat. Rev. Chem.*, 2017.

[4] D. Davidovikj *et al.*, "Nonlinear dynamic characterization of two-dimensional materials," *Nat. Commun.*, 2017.

[5] M. Radmacher, "Measuring the elastic properties of living cells by the atomic force microscope," *Methods Cell Biol.*, 2002.

[6] D. Kirmizis and S. Logothetidis, "Atomic force microscopy probing in the measurement of cell mechanics," *Int. J. Nanomed*, 2010.

[7] C.-Y. Hung *et al.*, "Adhesion measurement of micropatterned surfaces using three-dimensional-printed atomic force microscopy tips," *Jpn. J. Appl. Phys*, 2017.

[8] M. Lekka and J. Pabijan, "Measuring elastic properties of single cancer cells by afm," in *Atomic Force Microscopy*. Springer, 2019.

[9] P. de Pablo and I. Schaap, "Atomic force microscopy of viruses," in *Physical Virology*, pp. 159–179. Springer, 2019.

[10] E. Betzig *et al.*, "Combined shear force and near-field scanning optical microscopy," *Appl. Phys. Lett.*, 1992.

[11] M. Galluzzi *et al.*, "Space-resolved quantitative mechanical measurements of soft and supersoft materials by atomic force microscopy," *NPG Asia Mater.*, 2016.

[12] M. Lee *et al.*, "Noncontact friction via capillary shear interaction at nanoscale," *Nat. Commun.*, 2015.

[13] A. Humphris *et al.*, "Transverse dynamic force spectroscopy: a novel approach to determining the complex stiffness of a single molecule," *Langmuir*, 2002.

[14] M. Lee *et al.*, "Study of a nanoscale water cluster by atomic force microscopy," *Faraday Discuss.*, 2009.

[15] M.-D. Krass *et al.*, "Dynamic shear force microscopy of viscosity in nanometer-confined hexadecane layers," *J. Phys. Condens. Matter*, 2016.

[16] Y. Jeong *et al.*, "Direct tip-sample interaction force control for the dynamic mode atomic force microscopy," *Appl. Phys. Lett.*, 2006.

[17] K. S. Karvinen *et al.*, "Direct tip-sample force estimation for high-speed dynamic mode atomic force microscopy," *IEEE Trans Nanotechnol*, 2014.

[18] T. Nguyen *et al.*, "Estimation of the shear force in transverse dynamic force microscopy using a sliding mode observer," *AIP Advances*, 2015.

[19] T. Nguyen *et al.*, "Real-time sliding mode observer scheme for shear force estimation in a transverse dynamic force microscope," *Asian J. Control*, 2018.

[20] K. Zhang *et al.*, "A multimode transverse dynamic force microscope-design, identification and control," *IEEE Trans. Ind. Electron.*, 2019.

[21] A. F. Payam, D. Martin-Jimenez, and R. Garcia, "Force reconstruction from tapping mode force microscopy experiments," *Nanotechnology*, 2015.

[22] A. Labernadie *et al.*, "Protrusion force microscopy reveals oscillatory force generation and mechanosensing activity of human macrophage podosomes," *Nat. Commun.*, 2014.

[23] J. M. Fletcher *et al.*, "Self-assembling cages from coiled-coil peptide modules," *Science*, vol. 340, no. 6132, pp. 595–599, 2013.

[24] R. L. Harniman *et al.*, "Real-time tracking of metal nucleation via local perturbation of hydration layers," *Nat. Commun.*, vol. 8, no. 1, pp. 1–8, 2017.

[25] M. Antognozzi *et al.*, "Direct measurements of the extraordinary optical momentum and transverse spin-dependent force using a nano-cantilever," *Nat. Phys.*, vol. 12, no. 8, pp. 731–735, 2016.

[26] L. Huang and C. Su, "A torsional resonance mode afm for in-plane tip surface interactions," *Ultramicroscopy*, vol. 100, no. 3-4, pp. 277–285, 2004.

[27] M. Reinstädtler *et al.*, "Imaging and measurement of elasticity and friction using the trmode," *J. Phys. D Appl Phys*, vol. 38, no. 18, p. R269, 2005.

[28] M. Antognozzi, "Investigation of the shear force contrast mechanism in transverse dynamic force microscopy." Ph.D. dissertation, University of Bristol, 2000.

[29] B. Moore, "Principal component analysis in linear systems: Controllability, observability, and model reduction," *IEEE Trans. Autom. Control.*, 1981.

[30] C. Edwards and S. Spurgeon, *Sliding mode control: theory and applications*. Crc Press, 1998.

[31] M. N. Mahyuddin *et al.*, "Adaptive observer-based parameter estimation with application to road gradient and vehicle mass estimation," *IEEE Trans. Ind. Electron.*, 2013.

[32] M. Antognozzi *et al.*, "A new detection system for extremely small vertically mounted cantilevers," *Nanotechnology*, 2008.

[33] S. Kuiper *et al.*, "Integrated design of the feedback controller and topography estimator for atomic force microscopy," *Control Eng. Pract.*, 2013.

[34] K. Zhang *et al.*, "A super-twisting observer for atomic-force reconstruction in a probe microscope," *Control Eng. Pract.*, vol. 94, p. 104191, 2020.

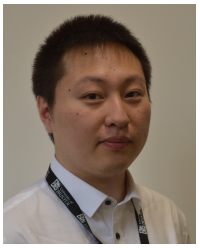

Kaiqiang Zhang received the B.Eng degree in automation & control from the School of Electronic and Information Engineering at the Xi'an Jiaotong University, China in 2012. He obtained the M.Sc. (dist.) in robotics and Ph.D. in control degrees in 2013 and 2019 respectively.

He was a control system engineer at the Institute of Microelectronics of the Chinese Academy of Sciences in 2014. During 2018-2019, he worked as a Research Associate in nuclear robotics at the University of Bristol, UK. He is now a Control Systems Engineer at the UK Atomic Energy Authority and a visiting Senior Research Associate at the University of Bristol. His research interests are on adaptive control, high precision control, system integration, and robotics.

Guido Herrmann received the degree 'Diplom-Ingenieur der Elektrotechnik' (Highest Hons) from the Technische Universitaet zu Berlin, Germany, and the Ph.D. degree from the University of Leicester, UK, in 2001.

From 2001 to 2003, he was a Senior Research Fellow with the A*Star Data Storage Institute, Singapore. From 2003-2007, he was a Research Associate, Research Fellow, and Lecturer at the University of Leicester. Between 2007-2019, he worked at the University of Bristol, U.K., as a Lecturer, Senior Lecturer, and Reader in Control and Dynamics. Since 2019, he is a Professor in Robotics at the University of Manchester. His research interests include the development and application of novel, robust and nonlinear controllers.

Dr. Herrmann is a Fellow of the IET and has been awarded with Dr. Jing Na the 2017 Hsue-shen Tsien Paper Award. He was the project lead of the EPSRC grants EP/I034882/1 & EP/I034831/1 associated with this publication.

Thang T. Nguyen received his B.Eng. and M.S. degrees in electrical engineering from Hanoi University of Technology, Hanoi, Vietnam, in 2002 and 2004 respectively, and his Ph.D. degree in electrical engineering from Rutgers University, NJ, USA, in 2010.

He was working as a Postdoctoral Research Associate at the Universities of Leicester and Exeter from 2012 until 2015. He is now an Assistant Professor at the Department of Engineering, Texas A&M University - Corpus Christi, USA. His research interests include optimization, optimal control, adaptive control, sliding mode control, atomic force microscopy and robotics.

Christopher Edwards received a B.Sc. (Hons) degree in mathematics from the University of Warwick, U.K., and a Ph.D. degree in control from the University of Leicester, Leicester, U.K., in 1995.

He is a Professor of control engineering with the College of Engineering, Mathematics and Physical Sciences, University of Exeter, U.K.. He is a co-author of 400 refereed papers in his areas of interest and of three books: Sliding Mode Control: Theory and Applications (Taylor & Francis, 1998), Fault Detection and Fault Tolerant Control using Sliding Modes (Springer-Verlag, 2011), and Sliding Mode Control and Observation (Birkhauser, 2013). In addition, he recently coedited the monograph Fault Tolerant Flight Control: A Benchmark Challenge (Springer-Verlag, 2010). His current research interests include sliding-mode control and observation and applications to fault detection and fault-tolerant control.

Dr. Edwards is currently Chair of the IEEE Technical Committee on Variable Structure Systems.

Massimo Antognozzi received the B.Sc. degree from the University of Bologna, Italy, and the Ph.D. degree from the University of Bristol, U.K.. He is currently a Senior Lecturer in Nano Physics at the School of Physics of the University of Bristol. His main research interest is to develop tools to investigate nanoscale systems. Together with Professor M. Miles, he is the inventor of the Transverse Dynamic Force Microscope.

Mervyn Miles (B.Sc., M.Sc., Ph.D.) was a Professor and is an Emeritus Professor of Physics at the University of Bristol and Royal Society Wolfson Research Merit Award Holder. Professor Miles was the initiator of the Centre of Nano Science and Quantum Information (NSQI), where much of the experimental research on the Transverse Dynamic Force Microscope has been carried out. Dr. Miles was elected as a fellow of the Royal Society, U.K., in 2011.